THE INFLUENCE OF TEMPERATURE ON GEOTHERMAL POWER PLANT PERFORMANCE BASED ON GEOLOGY IN HUANGSHADONG GEOTHERMAL FIELD, CHINA

by

Chao LUO[a], Lichang HUANG[b], Chaohui LIN[a*], Huiwen HUANG[a], and Huipeng ZENG[a]

[a] School of Architecture and Civil Engineering, Huizhou University, Huizhou, China
[b] School of Computer Science and Engineering, Huizhou University, Huizhou, China

Original scientific paper
https://doi.org/10.2298/TSCI221215079L

The geological structure is rather complicated in Guangdong province, in China. The 10 deep fault belts are mainly oriented in North-East. The North-East fault belts are good channels for deep thermal energy upwelling, which can form a geothermal water reservoir zone. The heating of atmospheric precipitation and surface water by deep rocks is the primary formation mechanism for the hydrothermal resources in the Huangshadong geothermal field. The results show that the two-stage conversion system of flash-binary is more reasonable when the geofluid temperature is higher than 130 °C. With every 10 °C increment of geofluid temperature for flash-binary system, the power output and exergy efficiency increase by 21.6-38.7% and 6.0-13.1%, respectively. The power output and exergy efficiency will decrease by about 20-40% when cooling temperature arising from 15 °C to 25 °C. The research will provide the basic data for the demonstration of geothermal resource exploitation.

Key words: *geothermal geology, power system, optimal design, thermodynamic, feasible proposal*

Introduction

Geothermal energy can be used as a heat source for energy conversion. It is mainly distributed at the junction of plates. The geothermal heat potential stored within the upper 5 km of the earth has been estimated as $1.4 \cdot 10^8$ EJ. Less than 1% of this resource has been developed yet 78 countries report using a combined total of $4.3 \cdot 10^5$ TJ direct geothermal heat [1]. The geothermal resources with temperatures higher than 130 °C are suitable for geothermal power generation [2]. In China, the annual utilization energy quality of hydrothermal geothermal resources is about $1.9 \cdot 10^9$ tonnes of standard coal [3]. The geothermal resources are abundant in Guangdong Province because of the influence of the movement of the Eurasian, Indian and Philippine Sea plates.

Geothermal power generation was first tested in Larderello geothermal field, Italy. A capacity of 250 kW geothermal power plant was successfully installed based on the test, which is the beginning of commercial geothermal power generation. Then, wet and dry steam geothermal power plants were built in Wailaki, New Zealand, and Geysers geothermal fields,

* Corresponding author, e-mail: luochao@hzu.edu.cn

USA, respectively [4, 5]. Geothermal power plants have a positive effect on carbon emission reduction for carbon neutrality. In China, most of the geothermal resources belong to hydrothermal type and the temperature is below 150 °C. As a result, the available geothermal power technologies mainly include flash, ORC, Karina cycle, and a combination of the technologies. At the end of 2021, the installed capacity of geothermal power plants in the world had reached 15950 MW, an increase of about 30% over 2015 [6]. In China, the installed capacity of geothermal power plants is about 47 MW by the end of 2021, of which the installed capacity of Yangbajing and Yangyi power plants in Tibet is 43.08 MW, accounting for 91.5% [7, 8]. Other power plants with small capacity are in trial operation, as shown in tab. 1.

Table 1. Operation geothermal power plants in China in 2019

No.	Location	Company	State	Capacity [MW]
1	Yangbajing, Tibet	Tibet Geothermal Company	Operation	24.18
2	Yangbajing, Tibet	China Longyuan Power Group Corporation, Limited	Operation	2.00
3	Yangyi, Tibet	China Longyuan Power Group Corporation, Limited	Operation	0.9
4	Yangyi, Tibet	Hangzhou Jinjiang Group, Zhejiang	Operation	16
4	Dehong, Yunnan	Zhengzhou Dimeite New Energy Technology Company	Operation	2.00
5	Huabei oilfield, Hebei	China National Petroleum Corporation	Operation	0.9
6	Kangding, Sichuan	Sichuan Kangsheng Geothermal Company	Operation	0.40
7	Gonghe, Qinghai	Qinghai Hydrological Institute	Operation	0.20
8	Ganzi, Sichuan	Sichuan Kangsheng Geothermal Company	Operation	0.2
	Total			46.78

The theoretical research on geothermal power system mainly focuses on thermal performance and economic simulation. The thermodynamic and mathematical performance of the different cooling systems for geothermal power plants at various climatic conditions were analysed in Turkey. The hybrid cooling systems can be determined at the operation periods for the geothermal power plants [9]. The thermodynamic performance can be further improved by introducing geothermal energy for a coal-fired power generation system. It is found that the generated power of geothermal energy is increased by1272 kW, the power generation exergy and thermal efficiencies of geothermal energy are enhanced by 29.1%and 6.0% [10]. The effect of climatic environment on ORC power system performance was evaluated, the water-cooling mode is preferred with better thermodynamic and economic performance for ORC [11]. Some research study a more efficient plant as well as multigeneration productions, the influence of geothermal water temperature, flash pressure, and ambient temperature on plant's performance are parametrically investigated. The integration of various systems with the geothermal power plant will be an increase in system performances [12]. A novel hybridization of a flash-binary geothermal cycle, a gas turbine cycle, and an organic flash is proposed. The net power of the proposed system at the base conditions is about 8016 kW and with 35.43% exergy efficiency. The air preheater effectiveness has the highest impact on sys-

tem performance from the view of heat transfer sensitivity analysis [13]. Four typical geothermal power system are proposed for low dryness hot dry rock geothermal fluid with 150-200 °C, the double stage flash combined ORC system has the best matching characteristics with geothermal fluids in terms of power generation performance [14]. Franco and Vaccaro [15] quantifies cost and efficiency factors and proposes a sustainability objective function, which will be applied in the design of geothermal power plants.

Most of the literature focus on high temperature geothermal resource. However, most geofluid temperature is less than 150 ℃ in China. The paper revealed the law between the distribution of geothermal hot spots and deep fault belts, and combined the subface feature with the surface utilization technology. The novelty of the paper is that it analyzed the effect of cooling water temperature on the thermodynamic performance of four geothermal power systems for typical hydrothermal resources in Huangshadong geothermal field, Guangdong Province, which provides the basic data for the demonstration of geothermal resource exploitation.

Geology background

The development of rock fault structures and neotectonic activities in Guangdong province are continuously intense due to the influence of plate movement, especially against the background of repeated activity of deep and major faults, which provide favorable external environmental conditions for the formation of Guangdong geothermal fields. Figure 1 shows the deep and major faults of Guangdong Province. The 10 deep fault belts are mainly oriented in North-East, and the 11 major fault belts are mainly oriented in East-West and North-West. The scales of North-East and East-West trending fault belts are large, which constitute the main structural framework in the area. The scale of North-West trending faults is relatively small, the formation of faults is generally late and they often cut North-East and East-West trending faults [16].

The North-East trending deep fault belts mainly include Wuchuan-Sihui, Enping-Xinfeng, and Lianhuashan fault belts. These deep and major fault belts are composed of large-scale ductile shear zones, dynamic thermal metamorphic zones and a series of brittle faults trending North-East. The characteristic of these North-East trending faults is compressive and torsional first and then extensional. They are regional active major faults deep in the crust to the mantle and are good channels for deep thermal energy upwelling. They can form a geothermal water reservoir zone with certain width at the fault belt, which is a regional thermal control fracture. The formation of the geothermal field may be influenced by the Early Cretaceous and Late Jurassic intrusive rocks, and the geothermal spots are more active in the Huangshadong geothermal field where the Late Jurassic intrusive rocks are distributed. There is obvious correlation between the geothermal reservoir and the intrusive rocks. The geothermal reservoir belongs to convective geothermal field. The East-West trending deep fault belts mainly include Fogang-Fengliang, Gaoyao-Huilai and Suixi fault belts. Many hot spots arranged in North-East direction show intense geological activity.

The exploitable amount of geofluid (down to 1000 m) in Guangdong Province is about 642000 m^3/d. There are 320 natural hot spots with temperatures higher than 30 ℃ in Guangdong Province. There are 66 geothermal fields (20.7%) with temperatures between 30 °C and 40 °C, 158 geothermal fields (49.5%) with temperatures between 40 °C and 60 °C, 84 geothermal fields (26.6%) with temperatures between 60 °C and 90 °C, and 12 geothermal fields (3.8%) with temperatures higher than 90 °C. The hot spots are presented in fig. 1.

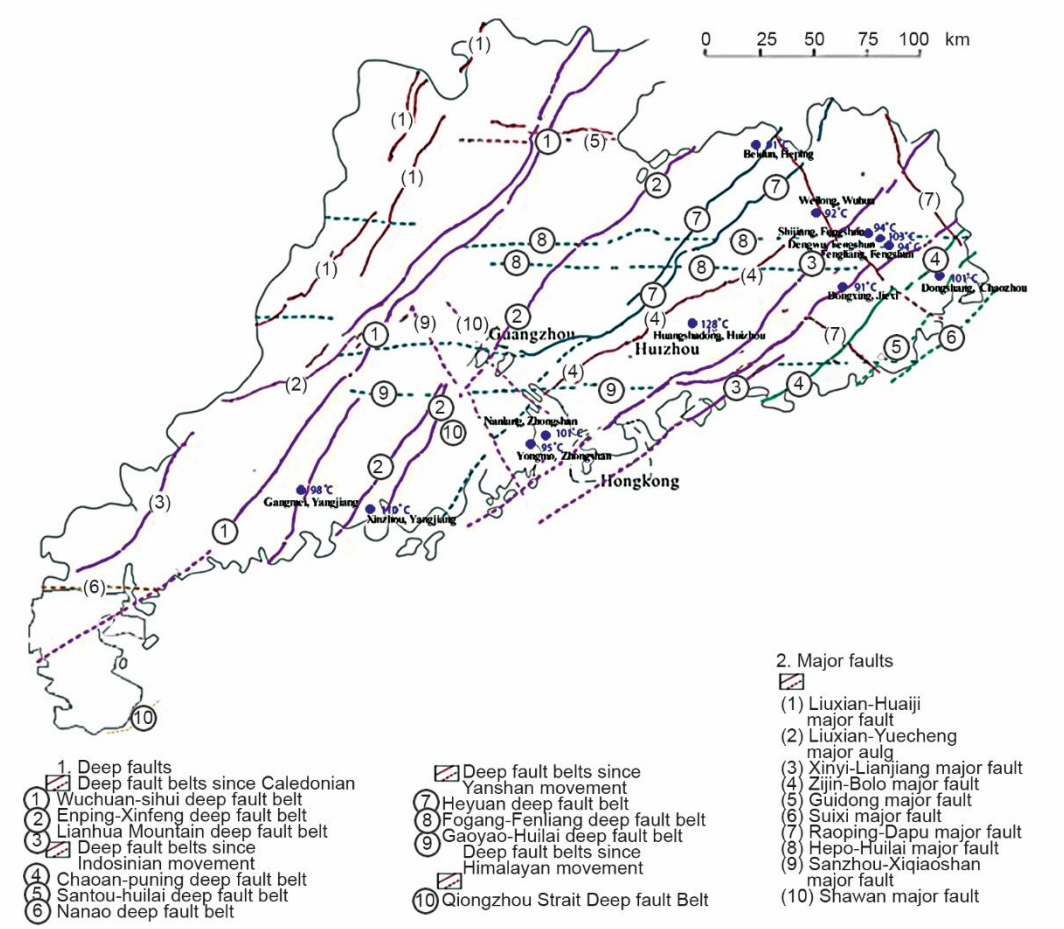

Figure 1. The deep and major faults of Guangdong Province

The hot spots are arranged along the deep regional faults, and about seventy-five percentage of the hot spots are arranged on the North-East or East-West trending faults, in the vicinity of the deep fault belts. The hot spots occurring in groups are always found at the junction of faults and the hot spots are distributed linearly. Table 2 lists the locations of geothermal water above 90 °C in Guangdong Province (blue dots in fig. 1).

Huangshadong geothermal field in Huizhou is a naturally exposed hot spot group, located on the southwest edge of Lianhua Mountain Range. Huangshadong geothermal field is in hilly terrain with high terrain in the north and low terrain in the south. The geofluid in Huangshadong is of hydrothermal characteristic, and mainly distributed in the contact belt between a magmatic rock body and the surrounding rock. The geothermal system is controlled by faults and late volcanic and magmatic activities. The formation mechanism of hydrothermal resources for the Huangshadong geothermal field can be described as follow: atmospheric precipitation, surface water or normal temperature groundwater infiltrates through faults and weathering fissures, and then absorbs normal or high rock heat in the deep circulation process of fault belts, and then rises and is naturally expose or is revealed by artificial engineering exposure. The geothermal resources in research area are affected by the orogenic belt-type heat

Table 2. The spot distribution of geothermal water above 90 °C in Guangdong Province

No.	Location	Wellhead temperature [°C]	Borehole temperature [°C]	Well depth [m]	Mineralization [gL^{-1}]
1	Huangshadong, Huizhou	118	127.7	2900	0.85-1.04
2	Xinzhou, Yangjiang	97	110.2	309	3.00
3	Dengwu, Fengshun	87	103	806	0.33
4	Dongshang, Chaozhou	82	101	227	1.12
5	Nanlang, Zhongshan	–	101	–	–
6	Gangmei, Yangjiang	–	97.8	–	–
7	Yongmo, Zhongshan	73-90	95	125	5.92
8	Shijiang, Fengshun	–	94.1	–	–
9	Fengliang, Fengshun	92	94	620	0.45
10	Weilong, Wuhua	82	91.8	100	0.89
11	Dongxing, Jiexi	83	91	100	0.53
12	Beidun, Heping	86	90.5	100	0.38

control tectonic system, which belongs to the plate boundary and the orogenic belt and the internal orogenic belt of the plate. Most of them are medium-high temperature geothermal resources, and the geothermal flow value is high, the average value is about 90-150 mW/m^2. The boundary conditions of the Huangshadong geothermal field are delineated based on water and heat-conducting structures and combination with topography and isotope geochemical characteristics, as shown in fig. 2.

The temperature of hydrothermal water in the Huangshadong geothermal field is relatively high (see below), the pH value of geothermal water is 6.92~8.95, and the total soluble solids content is 847~1037 mg/L. The water chemistry belongs to the HCO_3-Na type. There source temperature estimated by the potassium and magnesium temperature scale method is 105.8~116.8 °C, with an average of 111.3 °C. The temperature of thermal storage estimated by the silica temperature scale calculation method is 155.3~158.9 °C, with an average of 157.1 °C. The circulation depth of hydrothermal geothermal water is about 1000 m.

In the next section, a thermodynamic sensitivity analysis of the power system options for the Huangshadong geothermal field is presented. The following initial conditions of the hydrothermal geothermal water are estimated based on the geothermal well *Huire No 1* as shown in fig. 2: (1) the depth of the production well is 1000 m, (2) the temperature of geothermal water is 130 °C, and (3) the production rate of hot water is 150 t per hours.

System description and methodology

System description

The four physical models are single flash, double flash and ORC and flash-binary systems. Figure 3 shows the four physical models of the proposed systems.

For single and double flash system, the geothermal water is extracted from the production well, and then flows in to de separator. The geofluid is separated into saturated steam and water. The steam flows into the turbine and the saturated water is pumped to the rejection well.

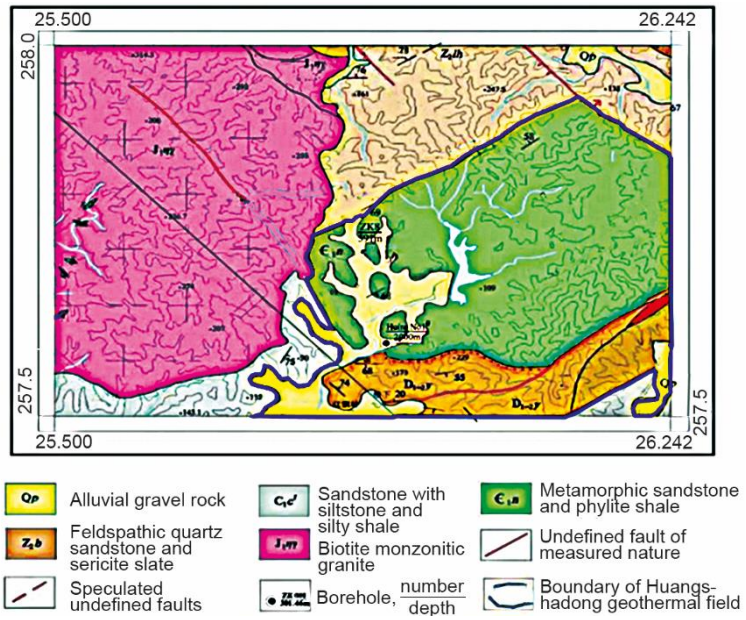

Figure 2. Huangshadong geothermal field boundary range map

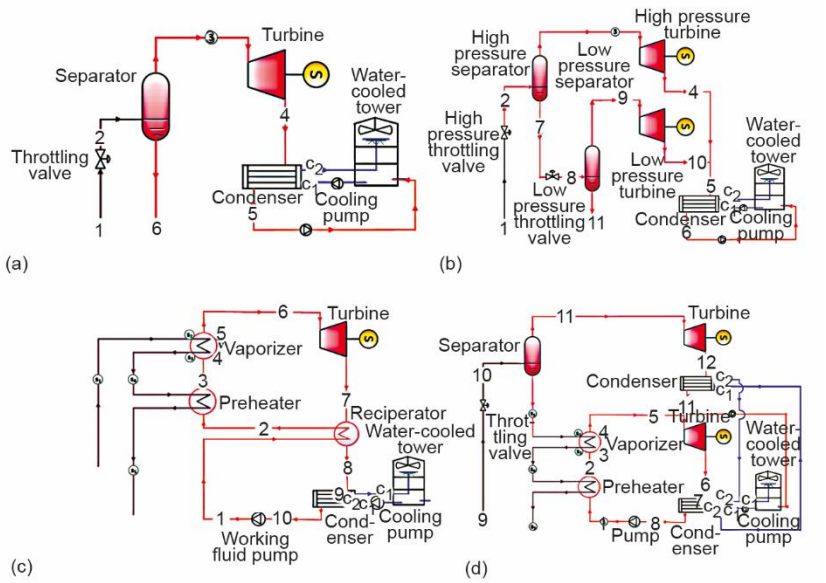

Figure 3. Process diagrams of systems; (a) single flash, (b) double flash, (c) ORC, and (d) flash-binary

For ORC. The geothermal water is an intermediate fluid in the cycle. The organic fluid exchange heat energy with geofluid in the vaporizer and preheater. The gas of organic fluid flows into the turbine and then cooled in the condenser. The geothermal water flows into

the injection well. The system was adopted indirect water-cooling method. A recuperator was used to improve the efficiency in the cycle.

For flash-binary system. It combined single flash and ORC. The process was the same as single flash system and ORC. However, the recuperator was not adopted in the ORC for the reason of simplification.

Methodology

The thermodynamic performance was simulated by eqs. (1)-(5).

$$\dot{m}_{\text{in}} = \sum \dot{m}_{\text{out}} \tag{1}$$

$$Q_{\text{in}} = W + \sum Q_{\text{out}} \tag{2}$$

$$\eta_1 = \frac{W_{\text{net}}}{\Delta Q} \tag{3}$$

$$\eta_2 = \frac{W_{\text{net}}}{E_{\text{in}}} \tag{4}$$

$$Ne = \frac{W_{\text{net}}}{3.6\dot{m}_{\text{in}}} \tag{5}$$

The optimization is a multi-objective, multi-variable problem. The initial parameters related to the system performance had to be defined, *i.e.* the heat source temperature and the mass flow rate. The optimum flash and evaporator pressure will be defined by maximizing the specific net power output, *Ne*.

Table 3 gives the related equations of the four systems. EXCEL was used to simulate the performance of the four systems.

Table 3. The mathematical model of components

Component	Single flash	Double flash	ORC	Flash-binary
Separator	$\dot{m}_1 = \dot{m}_3 + \dot{m}_6$ $\dot{m}_1 h_1 =$ $= \dot{m}_3 h_3 + \dot{m}_6 h_6$	$\dot{m}_1 = \dot{m}_3 + \dot{m}_7$ $\dot{m}_1 h_1 = \dot{m}_3 h_3 + \dot{m}_7 h_7$ $\dot{m}_7 = \dot{m}_9 + \dot{m}_{11}$ $\dot{m}_7 h_7 = \dot{m}_9 h_9 + \dot{m}_{11} h_{11}$	–	$\dot{m}_9 = \dot{m}_{11} + \dot{m}_{s1}$ $\dot{m}_9 h_9 = \dot{m}_{11} h_{11} + \dot{m}_{s1} h_{s1}$
Turbine for flash system	$\dot{m}_3 h_3 =$ $= \dot{m}_4 h_4 + W_{\text{flash}}$ $\eta_{\text{F,turbine}} =$ $= (h_3 - h_4)/(h_3 - h_{4,s})$	$\dot{m}_3 h_3 = \dot{m}_4 h_4 + W_{\text{turbine,1}}$ $\eta_{\text{turbine,1}} =$ $= (h_3 - h_4)/(h_3 - h_{4,s})$ $\dot{m}_9 h_9 = \dot{m}_{10} h_{10} + W_{\text{turbine,2}}$ $\eta_{\text{turbine,2}} =$ $= (h_9 - h_{10})/(h_9 - h_{10,s})$	–	$\dot{m}_{11} h_{11} = \dot{m}_{12} h_{12} + W_{\text{flash}}$ $\eta_{\text{F,turbine}} =$ $= (h_{11} - h_{12})/(h_{11} - h_{12,s})$
Condenser for flash system	$P_{\text{con}} = P_5$ $\dot{m}_4(h_4 - h_5) =$ $= \dot{m}_{C1}(h_{C2} - h_{C1})$	$P_{\text{con}} = P_5 = P_6$ $\dot{m}_5(h_5 - h_6) =$ $= \dot{m}_{C1}(h_{C2} - h_{C1})$	–	$P_{\text{con}} = P_{13}$ $\dot{m}_{12}(h_{12} - h_{13}) =$ $= \dot{m}_{C4}(h_{C5} - h_{C4})$
Condenser for ORC	–	–	–	$P_{\text{con}} = P_7 = P_8$ $\dot{m}_8(h_7 - h_8) =$ $= \dot{m}_{C2}(h_{C3} - h_{C2})$
Recuperator	–	–	$\dot{m}_f(h_1 + h_7) = \dot{m}_f(h_2 + h_8)$	

Thermodynamic performance analysis and discussion

Figure 4 gives the influence of $T_{heat,source}$ on maximum *Ne* and η_2 with different cooling water temperatures with single flash system. The maximum *Ne* and η_2 increase with the rising of $T_{heat,source}$. However, the slope of the curve is increasing in fig. 5(a), that is, the increment ratio between power output per unit geofluid and geofluid temperature is rising with the rising of $T_{heat,source}$, which means the *Ne* is more sensitive to geofluid temperature. The slope of the curve is decreasing in fig. 5(b), that is, the increment ratio between exergy efficiency and geofluid temperature decreases with the rising of $T_{heat,source}$, which means the η_2 is less sensitive to geofluid temperature. At the condition of cooling water temperature T_c of 25 °C, when the geofluid temperature rises from 80 °C to 90 °C, the increment of *Ne* and η_2 are 0.58 kWh per tonne and 2.90%, respectively. When the geofluid temperature rises from 140 to 150 °C, the increment of *Ne* and η_2 are 1.34 kWh per tonne and 1.36%, respectively.

The smaller the cooling water temperature is, the better are the maximum *Ne* and η_2. Under the condition of T_c of 15 °C, and with the $T_{heat,source}$ are 100 °C, 130 °C, and 150 °C, the maximum *Ne* are 3.183, 6.535, and 9.405 kWh per tonne, respectively, which are increased by 40.7%, 26.6% and 21.8%, respectively compared with those for cooling water temperature of 25 °C, The maximum η_2 are 25.9%, 30.49%, and 32.78%, respectively, which are increased by 41.0%, 26.7%, and 21.8%, respectively compared with those for cooling water temperature of 25 °C.

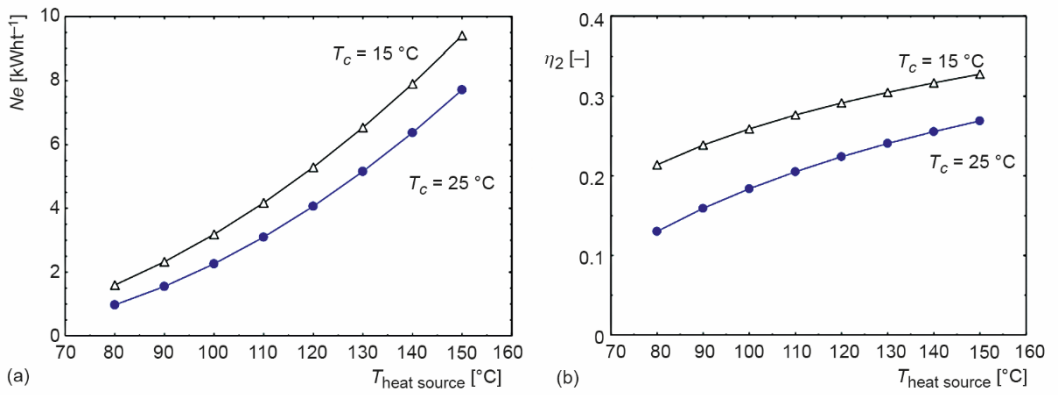

Figure 4. The effect of geofluid temperature on maximum *Ne* and η_2 of single system with different cooling water temperature; (a) *Ne* and (b) η_2

Figure 5 gives the influence of high pressure separator temperature T_2 and low pressure separator temperature T_8 on *Ne* with double flash system with $T_{heat,source}$ are 100 °C, 130 °C, and 150 °C, respectively. Under the condition of constant T_2, the *Ne* rises first and then declines with rising T_8. Under the condition of constant T_8, the *Ne* rises first and then declines with rising T_2. The calculated data explanate that with the $T_{heat,source}$ are 100 °C, 130 °C, and 150 °C, the maximum *Ne* are 2.96, 6.695, and 9.958 kWh per tonne, respectively, the maximum η_2 are 24.08%, 31.25%, and 34.72%, respectively, the optimum T_2 are 76.8 °C, 100 °C, and 108.7 °C, respectively, the optimum T_8 are 54.6 °C, 70.56 °C, and 69.5 °C, respectively. With the condition of $T_{heat,source}$ is 130 °C, the pressure value of high-pressure separator is great than 1 atmosphere, the volume of high-pressure separator will be reduced.

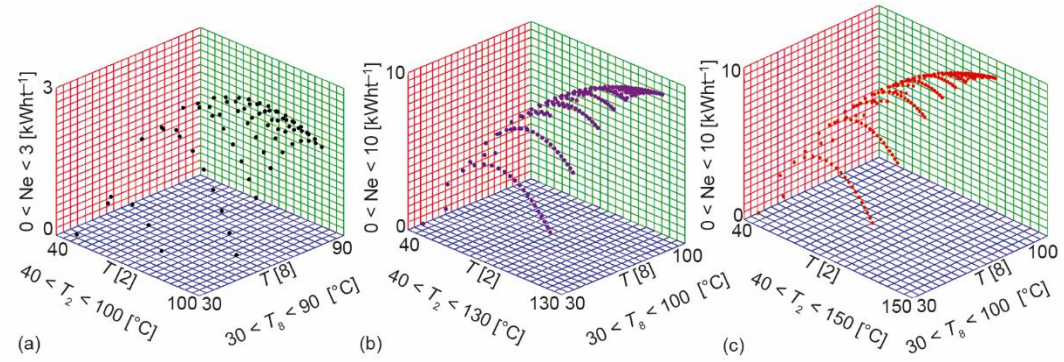

Figure 5. The relationship between *Ne* and separator temperature for double flash system; (a) $T_{heat,source}$ = 100 °C, (b) $T_{heat,source}$ = 130 °C, and (c) $T_{heat,source}$ = 150 °C

Figure 6 gives the influence of $T_{heat,source}$ on maximum *Ne* and η_2 with different cooling water temperatures for double flash power system. The maximum *Ne* and η_2 increase with the rising $T_{heat,source}$. Similar to the characteristic of the single flash system, the *Ne* is more sensitive to $T_{heat,source}$, and η_2 is less sensitive to $T_{heat,source}$. For a cooling water temperature of 25 °C, when the $T_{heat,source}$ rises from 80 °C to 90 °C, the increment of *Ne* and η_2 are 0.76 kWh per tonne and 3.77%, respectively. When the $T_{heat,source}$ rises from 140 °C to 150 °C, the increment of Ne and η_2 are 1.71 kWh per tonne and 1.64%, respectively.

The smaller the cooling water temperature is, the better are the maximum *Ne* and η_2. For a condition of cooling water temperature of 15 °C, and with the $T_{heat,source}$ are 100 °C, 130 °C, and 150 °C, the maximum *Ne* are 4.155, 8.452, and 12.09 kWh per tonne , respectively, which are increased by 40.4%, 26.2%, and 21.4%, respectively, compared with those for a cooling water temperature of 25 °C, and the maximum η_2 are 33.8%, 39.4%, and 42.1%, respectively, which are increased by 40.4%, 26.2%, and 21.3%, respectively compared with those for a cooling water temperature of 25 °C.

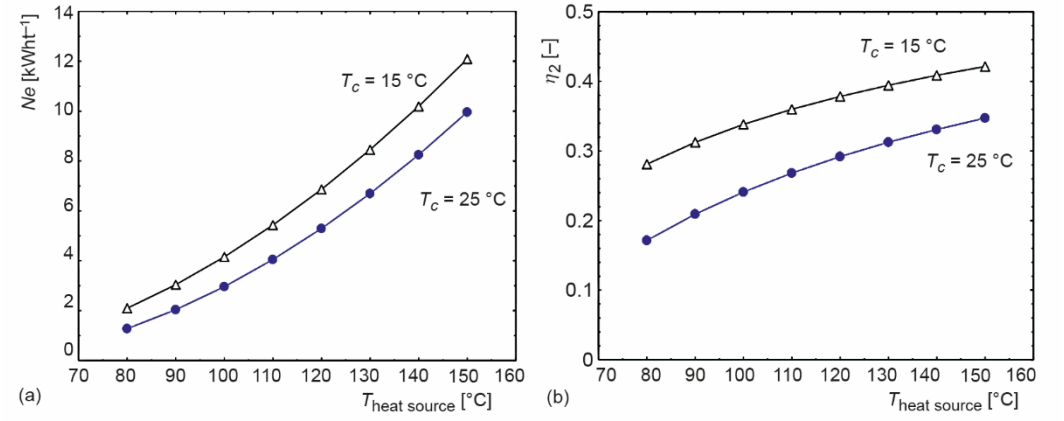

Figure 6. The effect of geofluid temperature on maximum *Ne* and η_2 of double system with different cooling water temperature; (a) *Ne* and (b) η_2

Figure 7 gives the influence of vaporizer temperature T_5 on *Ne* and η_2 for the ORC. Under the condition of constant $T_{heat,source}$, the *Ne* and η_2 rise first and then decline with the as-

cendant of T_5. When the *Ne* and η_2 get the maximum value, the T_5 is of a best value. With the $T_{heat,source}$ is 130 °C, the best value of T_5 is 86.02 °C, the *Ne* and η_2 get the maximum value of 5.205 kWh per tonne and 24.14%, respectively. The larger $T_{heat,source}$ is, the better are the *Ne* and η_2.

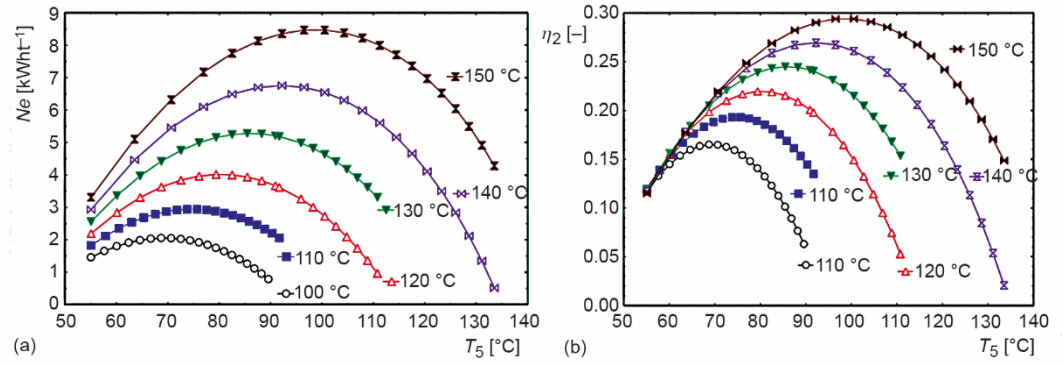

Figure 7. The influence of T_5 on *Ne* and η_2 of ORC; (a) *Ne* and (b) η_2

Figure 8 gives the effect of geofluid temperature on maximum *Ne*, η_1 and η_2 with different cooling water temperatures for binary power system. The maximum *Ne*, η_1 and η_2 increase with the rising of $T_{heat,source}$. Similar to the characteristic of the single flash system, the *Ne* is more sensitive to geofluid temperature, and η_1 and η_2 are less sensitive to geofluid temperature. Under the condition of cooling water temperature of 25 °C, with the geofluid temperature rises from 80 to 90 °C, the increment of *Ne* and η_2 are 0.56 kWh per tonne and 3.34%, respectively. When the geofluid temperature rises from 140 °C to 150 °C, the increment of *Ne* and η_2 are 1.61 kWh per tonne and 2.49%, respectively.

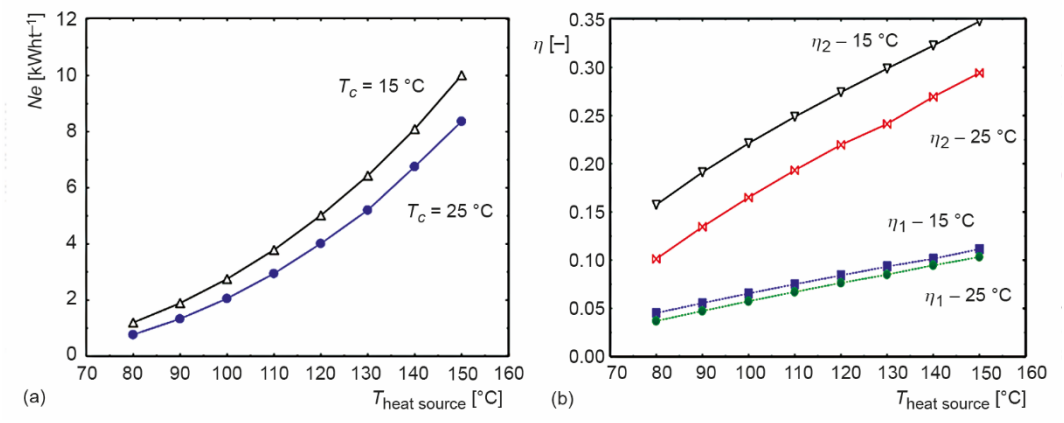

Figure 8. The effect of $T_{heat,source}$ on maximum *Ne*, η_1 and η_2 of binary power system with different cooling water temperature; (a) *Ne* and (b) η_2

The smaller the cooling water temperature is, the better are the maximum *Ne* and η_2. Under the condition of cooling water temperature of 15 °C, and with the $T_{heat,source}$ are 100 °C, 130 °C, and 150 °C, the maximum values of *Ne* are 2.749, 6.433, and 10.01 kWh per tonne,

respectively, which are increased by 34.0%, 23.6%, and 19.6%, respectively compared with that under the condition of cooling water temperature of 25 °C, and the maximum η_2 are 22.1%, 29.9%, and 34.7%, respectively, which are increased by 34.0%, 23.8%, and 17.9%, respectively compared with that under the condition of cooling water temperature of 25 °C.

Figure 9 gives the influence of geofluid temperature on maximum *Ne* and η_2 with different cooling water temperatures for flash-binary power system. The maximum *Ne* and η_2 increase with the rise of geofluid temperature. Similar to the characteristic of the single flash system, the *Ne* is more sensitive to geofluid temperature, and η_2 is less sensitive to geofluid temperature. For a cooling water temperature of 25 °C, when the geofluid temperature rises from 100 °C to 110 °C, the increment of *Ne* and η_2 are 1.07 kWh per tonne and 2.96%, respectively. When the geofluid temperature rises from 140 °C to 150 °C, the increment of *Ne* and η_2 are 1.76 kWh per tonne and 1.97%, respectively.

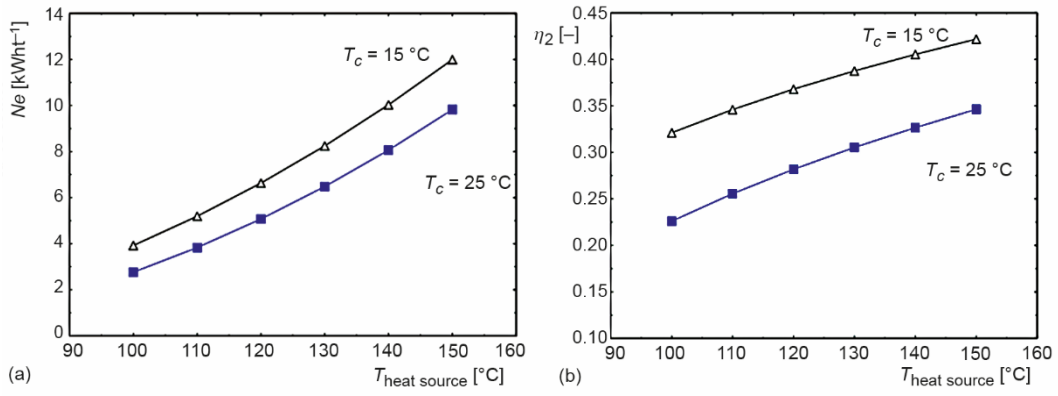

Figure 9. The effect of $T_{heat,source}$ on maximum *Ne* and η_2 of flash-binary power system with different cooling water temperature; (a) *Ne* and (b) η_2

The smaller the cooling water temperature is, the better are the maximum *Ne* and η_2. Under the condition of cooling water temperature of 15 °C, and with the $T_{heat,source}$ are 100 °C, 130 °C, and 150 °C, the maximum value of *Ne* are 3.922, 8.243, and 11.99 kWh per tonne, respectively, which are increased by 42.1%, 27.2%, and 22.1%, respectively, compared with that under the condition of cooling water temperature of 25 °C, and the maximum η_2 are 32.1%, 38.8%, and 42.2%, respectively, which are increased by 42.1%, 26.9%, and 21.8%, respectively, compared with those for a cooling water temperature of 25 °C.

The proposal of power plant construction

It is suitable to adopt the flash-binary power system in Huangshadong geothermal field. The indirect cooling water system should be used for the power system. The installed capacity of the power system is about 1 MW. The mass flow rate and temperature of geofluid are 150 tonn per hours and 130 °C, respectively. The mass flow rate and temperature of cooling water are 605 tonn per hours and 25 °C, respectively. The sub-flash and rejection temperature of power system are 100.3 °C and 70.6 °C, respectively. The power output per unit geofluid is 6.5 kWh per tonne. The thermal and exergy efficiency are 9.4% and 30.5%, respectively.

Conclusions

The formation mechanism of hydrothermal resources for the Huangshadong geothermal field is analyzed based on the geological background. Four geothermal power systems are considered for the Huangshadong geothermal field. The conclusions are as follows.

- There are mainly 10 deep fracture zones and 11 large fracture zones in Huizhou city, Guangdong province, China. The deep fracture structures distributed in North-East, and the large fracture structures distributed in East-West and North-West. The hot spots occurring in groups are found always at the junction of faults and the hot spots distributed along with deep fracture. The heating of atmospheric precipitation and surface water by deep rocks is the primary formation mechanism for the hydrothermal resources in the Huangshadong geothermal field.
- The thermodynamic performance of two-stage conversion systems is better than that of ORC and single flash systems. The two-stage conversion system of flash-binary is more reasonable when the geofluid temperature is higher than 130 °C.
- The geofluid temperature has greater effect on power output compared with exergy efficiency. With every 10 °C increment of geofluid temperature for flash-binary system, the power output and exergy efficiency increase by 21.6-38.7% and 6.0-13.1%, respectively.
- The cooling water temperature has an important influence on system performance. The power output and exergy efficiency will decrease by about 20-40% when cooling temperature arising from 15 to 25 °C.

Acknowledgment

This work is supported by the Indigenous Innovation's Capability Development Program of Huizhou University (HZU202002), Online Open Courses Steering Committee of Guangdong Undergraduate Universities (2022ZXKC437), the Huizhou University Key Academic Discipline Project and the State Key Laboratory of Subtropical Building Science (Grant No.2018ZB08)..

Nomenclature

E_{in} – exergy rate of geothermal fluid, [kW]
$\dot{m}_{in}$ – mass-flow rate of inlet geofluid, [kWht^{-1}]
$\dot{m}_{out}$ – mass-flow rate of outlet geofluid, [kWht^{-1}]
Ne – power output per unit geofluid, [kWht^{-1}]
Q_{in} – heat input energy, [kJs^{-1}]
Q_{out} – output heat energy, [kJs^{-1}]
T_2 – high pressure separator temperature, [°C]
T_8 – low pressure separator temperature, [°C]
T_c – cooling water temperature, [°C]
T_{flash} – flash temperature, [°C]
$T_{heat,source}$ – geofluid temperature, [°C]
W – output useful work of the system, [kW]
W_{net} – net power output of the system, [kW]
ΔQ – circulating heating energy of geothermal fluid, [kW]

Greek symbols

η_1 – thermal efficiency, [%]
η_2 – exergy efficiency, [%]

References

[1] Charlotte, A. A., *et al*., Unlocking the UK Geothermal Resource Base, *Proceedings*, World Geothermal Congress, Reykjavik, Iceland, 2020
[2] Stefansson, V., World geothermal assessment *Proceedings*, World Geothermal Congress, Antalya, Turkey, 2005
[3] Zhang, L., *et al.,* Geothermal Power Generation in China: Status and Prospects, *Energy Science & Engineering, 7* (2019), 5, pp. 1428-1450
[4] Parri, R., Lazzeri, F., *Geothermal Power Generation*, Woodhead Publishing, Sawoton, UK, 2016, pp. 537-590

[5] Dipippo, R., Geothermal Power Plants: Evolution and Performance Assessments, *Geothermics, 53* (2015), 11, pp. 291-307
[6] Huttrer, G. W., Geothermal Power Generation in the World 2015-2020 Update Report, *Proceedings,* World Geothermal Congress, Reykjavik, Iceland, 2020
[7] Wang, Y. Z., *et al.*, The Above-Ground Strategies to Approach the Goal of Geothermal Power Generation in China: State of Art and Future Researches, *Renewable and Sustainable Energy Reviews, 138* (2021), Mar., pp. 1364-0321
[8] Tian, T. S., *et al.,* Rapid Development of China's Geothermal Industry - China National Report of the 2020 World Geothermal Conferencee, *Proceedings,* World Geothermal Congress, Reykjavik, Iceland, 2021
[9] Basaran, T., *et al.,* Thermodynamic and Mathematical Analysis of Geothermal Power Plants Operating in Different Climatic Conditions, *Case Studies in Thermal Engineering, 30* (2022), 101727
[10] Zhang H., *et al.,* Thermodynamic Performance Analysis of an Improved Coal-Fired Power Generation System Coupled with geothermal Energy Based on Organic Rankine Cycle, *Renewable Energy, 201* (2022), Dec., pp. 273-290
[11] Li, J, *et al.,* Influences of Climatic Environment on the Geothermal Power Generation Potential, *Energy Conversion and Management, 268* (2022), 115980
[12] Yilmaz, F., *et al.,* Modeling and Design of the New Combined Double-Flash and Binary Geothermal Power Plant for Multigeneration Purposes; Thermodynamic Analysis, *International Journal of Hydrogen Energy, 47* (2022), 45, pp. 19381-19396
[13] Zhang, L., Sobhani, B., Comprehensive Economic Analysis and Multi-Objective Optimization of an Integrated Power and Freshwater Generation Cycle Based on Flash-Binary Geothermal and Gas Turbine Cycles, *Journal of Cleaner Production, 364* (2022), 132644
[14] Li, T., *et al.,* Thermodynamic, Economic, and Environmental Performance Comparison of Typical Geothermal Power Generation Systems Driven by Hot Dry Rock, *Energy Reports, 8* (2022), Nov., pp. 2762-2777
[15] Franco, A., Vaccaro, M. A., Combined Energetic and Economic Approach for the Sustainable Design of Geothermal Plants, *Energy Conversion and Management, 87* (2014), Nov., pp. 735-745
[16] Li, J. X., *et al.,* Evaluation of Mineral-Aqueous Chemical Equilibria of Felsic Reservoirs with Low-Medium Temperature: A Comparative Study in Yangbajing Geothermal Field and Guangdong Geothermal Fields, *Journal of Volcanology and Geothermal Research, 352* (2018), Feb., pp. 92-105

Paper submitted: December 15, 2022
Paper revised: February 22, 2023
Paper accepted: March 7, 2023
© 2023 Society of Thermal Engineers of Serbia.
Published by the Vinča Institute of Nuclear Sciences, Belgrade, Serbia.
This is an open access article distributed under the CC BY-NC-ND 4.0 terms and conditions.